Overview of Computational and Analytical Modeling of Particle Transport and Deposition in Turbulent Flows

Goodarz Ahmadi[1]

The mechanics of aerosol motions in turbulent flows is reviewed, and the forces responsible for migration, dispersion and wall deposition of particles are discussed. Recent computational procedures for studying deposition of aerosols from turbulent air streams on smooth and rough surfaces are reviewed. These include a nonlinear rate-dependent algebraic stress turbulence model for simulating the mean flow, as well as the directional turbulence intensities in complex domains. Approximate and exact (direct simulation) methodologies for digital simulation of instantaneous fluctuating velocity components in a turbulent air stream are described. Effects of Brownian diffusion, Saffman lift force and gravity are included in the particle equation of motion. The procedure for simulating the Brownian motion of submicron particles is also discussed. Examples of deposition of aerosol particles in the range of 0.01 to 10 microns from initially uniform concentrations and point sources are presented.

A recently developed model for particle deposition rate, which is based on the coherent vortical structure of turbulent near wall flows, is described. It is shown that the model predictions for smooth and rough surfaces are in reasonable agreement with the digital simulation results and the experimental data. Certain results concerning wall deposition of charged particles and nonspherical particles are also presented.

INTRODUCTION

Understanding the transport and deposition processes of particles in the atmosphere and various air passages is of crucial interest to the fields of environmental science, atmospheric science and numerous industrial applications. The need of microelectronic industries for controlling microcontamination by small particles has motivated a number of recent studies on mechanics of aerosol motions. Cooper [1] provided an excellent review of the needed microcontamination control research for microelectronic industries. Progress in analyzing particles deposition rate on wafers was reported by Cooper et al. [2] and Liu and Kang-ho [3]. Diffusion of particles in laminar flows is relatively well understood. An extensive review on the subject was provided by Levich [4]. In most practical industrial and environmental applications, however, the air stream is turbulent and particles are transported by the mean motion and are dispersed by turbulence fluctuations and Brownian diffusion. In addition, electrostatic and gravitational forces could significantly affect the particle dispersion and wall deposition processes. Fuchs [5], Davies [6], Friedlander and Johnstone [7], Cleaver and Yates [8] and Fichman et al. [9] provided semi-empirical expressions for particle mass flux from a turbulent stream to smooth surfaces. Particle deposition on rough walls was studied by Browne [10] and Wood [11]. Extensive reviews on the subject were provided by Wood [12], Hidy [13] and Papavergos and Hedley [14].

Use of computer simulation for analyzing

1. Department of Mechanical and Aeronautical Engineering, Clarkson University, Postdam, NY 13699.
Scientia Iranica, Vol. 1, No. 1, © Sharif University of Technology, April 1994.

aerosol dispersion was suggested by several authors. Ahmadi and Goldschmidt [15] used digital simulation and analytical techniques to study the turbulent dispersion of small spherical particles. Peskin [16] considered turbulent diffusion of particles in a channel flow. Dispersion of small particles in a numerically simulated random isotropic field was studied by Ounis and Ahmadi [17, 18] and Maxey [19]. McLaughlin [20] and Ounis, Ahmadi and McLaughlin [21, 22] analyzed the trajectories of rigid spherical particles in a channel flow and their wall deposition rates using a pseudo-spectral computer code to simulate the instantaneous turbulent flow field. Rizk and Elghobashi [23] analyzed motions of particles suspended in a turbulent flow near a plane wall. Abuzeid, Busnaina and Ahmadi [24, 25] and Li and Ahmadi [26] used a simple simulation technique to study the dispersion and deposition processes of suspended particles released from point sources in turbulent channel flows. Recently, Li and Ahmadi [27, 28] simulated the deposition velocity of aerosol of various sizes for smooth and rough surfaces in turbulent flows. Deposition of particles in complex geometry air passages was studied by Li et al. [29].

In spite of numerous studies, the mechanisms that control the wall deposition of particles from turbulent flows is not well understood. Most earlier models for particle deposition rate are based on the free-flight concept of Friedlander and Johnstone [7]. Accordingly, the particles are transported by turbulence fluctuation to regions very near the wall. Particles that reach to their stopping distance (subject to certain initial velocity) are assumed to be deposited on the surface by the free-flight mechanism. The credibility of this model has now been severely questioned. Cleaver and Yates [8], Fichman et al. [9] and, more recently, Fan and Ahmadi [30], developed the sublayer model for particle deposition rate which is based on the coherent structure of near wall turbulence. The model was extended to rough surfaces and the presence of electrostatic and gravitational forces by Fan and Ahmadi [30, 31]. Good agreement of the model predictions with the digital simulation results and the experimental data was also reported.

In this work, the recently developed digital simulation methodology for analyzing the deposition rate of fine particles on smooth and rough surfaces from turbulent air streams is reviewed. The procedure for simulating the instantaneous turbulent velocity field is described. The governing equation of motion of aerosol particles which includes the Brownian diffusion and the turbulent dispersion effects, in addition to the gravitational, the Saffman lift and electrostatic forces is presented.

The procedure for simulating the instantaneous turbulent flow field using a nonlinear two-equation model is described. A computationally efficient method for simulating the Brownian motion of submicron particles is also discussed. Simulation results concerning deposition of aerosol particles in the range of 0.01 to 10 microns from initially uniform concentrations and point sources in turbulent flows are presented. Comparisons of simulation results with the available experimental data and those obtained from empirical equations are also performed. Effects of an electrostatic field on charged aerosols dispersion and deposition are discussed. Simulation results for dispersion and deposition of elongated ellipsoidal particles are also presented.

The foundation of the sublayer model for particle deposition from turbulent flows is reviewed and sample results are presented. Applications of the simulation methodology and the sublayer model to practical applications are discussed.

PARTICLE EQUATION OF MOTION

The equation of motion of a small aerosol particle is given by

$$\frac{du_i^p}{dt} = \frac{36\nu}{d^2(2S+1)C_c}(u_i - u_i^p)$$

$$+\frac{2K\nu^{\frac{1}{2}}d_{ij}}{Sd(d_{lk}d_{kl})^{\frac{1}{4}}}(u_j-u_j^p)$$

$$+(1-\frac{1}{S})g_i+n_i(t)+\frac{F_e}{m}, \quad (1)$$

and

$$\frac{dx_i}{dt}=u_i^p, \quad (2)$$

where, u_i^p is the velocity of the particle, x_i is its position, t is the time, d is the particle diameter, S is the ratio of particle density to fluid density, g_i is the acceleration of body force, $n_i(t)$ is the Brownian force per unit mass, F_e is the electrostatic force, m is the mass of the particle, ν is the kinematic viscosity, $K=2.594$ is the constant coefficient of Saffman's lift force, and u_i is the instantaneous fluid velocity with $u_i=\bar{u}_i+u_i'$, where $\bar{u}_i$ is the mean velocity of the fluid, and u_i' is the fluctuation component of fluid velocity. In Equation 1, C_c is the Stokes-Cunningham slip correction given as

$$C_c=1+\frac{2\lambda}{d}(1.257+0.4e^{-1.1d/2\lambda}), \quad (3)$$

where λ is the molecular mean free path of the gas, and d_{ij} is the deformation rate tensor.

The first term on the right hand side of Equation 1 is the drag force due to the relative motion between particles and fluid. The second term is the generalized Saffman [32] lift force. The third and the fourth terms are the gravitational and the Brownian forces. The last term is the electrostatic force. The drag force is always present and is generally a dominating force. Saffman lift force becomes important for particles which are not too small in the regions with a strong shear field.

The Brownian force, which is important for submicron particles, is modeled as a Gaussian white noise random process. The simulation procedure for the Brownian excitations was described in [21, 26]. Equation 1 requires the knowledge of the instantaneous fluid velocity field. The mean flow field is evaluated by using a nonlinear rate-dependent turbulence model. The instantaneous turbulent fluctuating velocities are approximated as continuous anisotropic Gaussian random fields. The simulation procedures are outlined in the subsequent sections.

MEAN FLOW SIMULATION PROCEDURE

The two-equation $k-\epsilon$ model is widely used in industrial applications due to its simplicity and the relative ease with which it could be incorporated in the Navier-Stokes equation solver codes. However, it is also well known that the standard $k-\epsilon$ model suffers from several serious shortcomings. Among the obvious ones are its inability to handle unequal turbulent normal stresses and its limitation in using an isotropic eddy viscosity. Rodi [33] developed an algebraic stress model that led to anisotropic eddy viscosity and offered certain improvements. Speziale [34] suggested a nonlinear expression for the turbulent stress tensor that satisfies the required invariance properties. Using a multiple scale direct interaction approximation, a similar expression was obtained by Yoshizawa [35, 36]. Chowdhury and Ahmadi [37] used an iterative solution of the stress transport model and obtained a similar rate-dependent algebraic expression for the turbulent stress tensor. A thermodynamically consistent rate-dependent model for turbulence was developed by Ahmadi [38] and Chowdhury and Ahmadi [39].

For an incompressible fluid, the equations of continuity and balance of momentum for the mean motion are given as

$$\frac{\partial\bar{u}_i}{\partial x_i}=0, \quad (4)$$

$$\frac{\partial\bar{u}_i}{\partial t}+\bar{u}_j\frac{\partial\bar{u}_i}{\partial x_j}=-\frac{1}{\rho}\frac{\partial\bar{p}}{\partial x_i}+\nu\frac{\partial^2\bar{u}_i}{\partial x_j\partial x_j}$$

$$-\frac{\partial}{\partial x_j}R_{ij}, \tag{5}$$

where $\bar{p}$ is the mean pressure, ρ is the constant mass density, and R_{ij} is the Reynolds stress tensor (second moment of fluctuation velocity). The thermodynamically consistent anisotropic expression for the Reynolds stress tensor as obtained in [38] is given as

$$R_{ij}=\frac{2}{3}k\delta_{ij}-2\nu^T\bar{d}_{ij}-\nu^T\frac{k}{\epsilon}[\alpha\frac{\hat{D}}{Dt}\bar{d}_{ij} +\gamma\frac{k}{\epsilon}\bar{d}_{lk}\bar{d}_{kl}\bar{d}_{ij}-\beta(\bar{d}_{ik}\bar{d}_{jk}-\frac{1}{3}\bar{d}_{kl}\bar{d}_{kl}\delta_{ij})], \tag{6}$$

where k is the turbulence kinetic energy, ν^T the turbulent eddy viscosity, ϵ is the energy dissipation rate and α, β and γ are certain constants. Here,

$$\frac{\hat{D}}{Dt}\bar{d}_{ij}=\frac{\partial}{\partial t}\bar{d}_{ij}+\bar{u}_k\frac{\partial\bar{d}_{ij}}{\partial x_k}+\bar{d}_{ik}\bar{\omega}_{kj}+\bar{d}_{jk}\bar{\omega}_{ki}, \tag{7}$$

is the co-rotational (Jaumann) derivative of the deformation rate tensor, and the mean deformation rate and the mean spin tensors are, respectively, defined as

$$\bar{d}_{ij}=\frac{1}{2}(\frac{\partial\bar{u}_i}{\partial x_i}+\frac{\partial\bar{u}_j}{\partial x_i}),\bar{\omega}_{jk}=\frac{1}{2}(\frac{\partial\bar{u}_j}{\partial x_k}-\frac{\partial\bar{u}_k}{\partial x_j}), \tag{8}$$

The eddy viscosity ν^T is given by

$$\nu^T=C^\mu k^2/\epsilon, \tag{9}$$

where C^μ is a constant.

The equations governing the kinetic energy of turbulence and the dissipation rate are

$$\frac{\partial k}{\partial t}+\bar{u}_j\frac{\partial k}{\partial x_j}=\frac{\partial}{\partial x_j}[(\nu+\frac{\nu^T}{\sigma^k})\frac{\partial k}{\partial x_j}] -R_{ij}\frac{\partial\bar{u}_i}{\partial x_j}-\epsilon, \tag{10}$$

$$\frac{\partial\epsilon}{\partial t}+\bar{u}_j\frac{\partial\epsilon}{\partial x_j}=\frac{\partial}{\partial x_j}[(\nu+\frac{\nu^T}{\sigma^\epsilon})\frac{\partial\epsilon}{\partial x_j}] -C^{\epsilon1}\frac{\epsilon}{k}R_{ij}\frac{\partial\bar{u}_i}{\partial x_j}-C^{\epsilon2}\frac{\epsilon^2}{k}. \tag{11}$$

The values of constants are given as

$$C^\mu=0.09,\sigma^k=1,\sigma^\epsilon=1.3, \tag{12}$$
$$C^{\epsilon1}=1.44,C^{\epsilon2}=1.92,$$

$$\alpha=0.93,\beta=0.54,\gamma=\frac{\beta^2}{48}=0.006. \tag{13}$$

This thermodynamically consistent model leads to an anisotropic effective viscosity and is capable of predicting the expected turbulence normal stress differences. In [36, 38], it was reported that the mean flow properties, including mean-square fluctuation velocity components, as predicted by this new model are in good agreement with the experimental data for a number of turbulent flows.

For simulating particle deposition processes, the fluctuation of turbulence perpendicular to the wall plays a crucial role. Therefore, the computational model must have the capability of accurately predicting the components of turbulence intensity. Thus, a simple $k-\epsilon$ model, which is associated with an isotropic assumption, is inherently incapable of providing the needed information.

The requirements of the anisotropic rate-dependent turbulent model were incorporated in the STARPIC - RATE computational model which was described at length in [36-38].

SIMULATION OF FLUCTUATION FLOW FIELD

For analyzing particle dispersion in a turbulent flow field, the instantaneous components of fluid velocity u_i are needed. As noted before, the mean velocity and the mean fluctuation kinetic energy may be obtained by the use of a conventional turbulence model, analytical expressions

and/or from experimental data. The instantaneous turbulence fluctuating motions, however, are random functions of space and time. The Monte-Carlo velocity simulation techniques have been used as a simple and economical method for generating time histories that have the random character and statistical properties of turbulence. According to Batchelor [40], turbulence fluctuations are nearly Gaussian processes for homogeneous flows. Kraichnan [41] suggested a simple method for generating a Gaussian random field which resembles a pseudo-isotropic turbulence. Accordingly, the instantaneous fluctuating velocity is given as

$$\vec{u}^{I*}(\vec{x}^*,t^*) = \sqrt{\frac{2}{N}}\{\sum_{n=1}^{N} \vec{u}_1(\vec{k}_n)\cos(\vec{k}_n\cdot\vec{x}^* + \omega_n t^*) + \sum_{n=1}^{N} \vec{u}_2(\vec{k}_n)\sin(\vec{k}_n\cdot\vec{x}^* + \omega_n t^*)\}. \quad (14)$$

In this equation,

$$\vec{u}_1(\vec{k}_n) = \vec{\zeta}_n \times \vec{k}_n, \qquad \vec{u}_2(\vec{k}_n) = \vec{\xi}_n \times \vec{k}_n, \quad (15)$$

with

$$\vec{k}_n\cdot\vec{u}_1(\vec{k}_n) = \vec{k}_n\cdot\vec{u}_2(\vec{k}_n) = 0, \quad (16)$$

which insure the incompressibility condition. The components of vectors $\vec{\zeta}_n$ and $\vec{\xi}_n$ and the frequencies ω_n are picked independently from a Gaussian distribution with a standard deviation of unity. Each component of $\vec{k}_n$ is a Gaussian random number with a standard deviation of 1/2. Here, N is the number of terms in the series.

In Equation 14, the dimensionless quantities are defined as

$$x^* = \frac{x}{l_o}, t^* = \frac{t}{t_o}, u_i^{I*} = \frac{u_i^{I'}}{u_i^*}, \quad (17)$$

where l_o, t_o and u_i^* are local scales of turbulence and $u_i^{I'}$ is the fluctuation fluid velocity which is assumed to be isotropic. For this pseudo-turbulent velocity field the energy spectrum $E(k)$ is given as

$$E(\kappa) = 16(2/\pi)^{1/2}\kappa^4 e^{-2\kappa^2}, \quad (18)$$

where κ is the wave number.

The experimentally measured root-mean-square (RMS) fluctuation velocities are generally anisotropic. Li and Ahmadi [26-29] used the experimental data of Kreplin and Eckelmann [42] and the results of the STARPIC-RATE and modified the fluctuation velocity given by Equation 14 in order to make it suitable for generating the nonisotropic instantaneous turbulent velocity field. Accordingly,

$$u_i' = u_i^{I'} e_i(y), \text{(no sum on i)} \quad (19)$$

where $e_1(y) = \sqrt{u'^2}/u^*$, $e_2(y) = \sqrt{v'^2}/u^*$, $e_3(y) = \sqrt{\omega'^2}/u^*$, are, respectively, the shape functions for the axial, vertical and transverse RMS velocities. Here, all intensities are nondimensionalized with respect to the shear velocity, $u^* = \sqrt{\tau_o/\rho}$, where τ_o is the wall shear stress which is related to the friction factor f, i. e.,

$$f = \frac{4\tau_0}{\frac{1}{2}\rho V^2} = \frac{8u^{*2}}{V^2}, \quad (20)$$

An empirical Equation [43] for the friction factor given by

$$\frac{1}{f^{\frac{1}{2}}} = -1.8\log[\frac{6.9}{2Re} + (\frac{k/h}{14.8})^{1.11}], \quad (21)$$

was used in [26-28]. In Equation 21, k is the roughness of the wall and $k = 0$ for a smooth wall.

Normal components of turbulence fluctuations near a wall has a profound effect on the

deposition rate of particles. Therefore, the magnitude of $e_2(y)$ must be correctly evaluated for small values of y. It is well known [44] that v' has a quadratic variation at short distances from the wall, i. e.,

$$v' \sim y^2 \qquad as \;\; y^+ \to 0. \tag{22}$$

In this study

$$e_2(y) = Ay^{+2} \qquad as \;\; y^+ < 2. \tag{23}$$

A value of $A = 0.0278$ was used in [26] in order to match the data of [42]. Here

$$y^+ = yu^*/\nu, \tag{24}$$

is the distance from the wall in wall units and $\nu = \mu/\rho$ is the kinematic viscosity of fluid.

Estimates for the length and time scales of turbulence for wall bounded flows were provided in [45]. These are

$$l_o = 0.1h(2Re)^{-1/8}, \tag{25}$$

and

$$t_o = \frac{l_o}{u^*} = \frac{2h}{20u^*(2Re)^{1/8}} = \frac{h}{2V}. \tag{26}$$

Equations 14 and 19 with $N = 100$ were used in [26-29] for simulating the fluctuation components of turbulent velocity in a straight channel and/or complex geometry flow passages. Sample space and time variations of fluctuation velocity components shown in [26] showed the random characters of real fluctuation velocity vector in real turbulent fields.

An alternative simpler method for simulating the fluctuating turbulent field was suggested by Abuzeid, Busnaina and Ahmadi [24, 25]. They used a simple Gaussian noise model which has a small correlation time of the order of Δt. Certain adjustments for making the model nonisotropic near a wall was also introduced. The model of Li and Ahmadi [26-28] which leads to smoothly varying Gaussian model has a more appropriate longer correlation time and its spectral behavior as given by Equation 18 is more representative of a real turbulent flow. The method of Abuzeid et al. [24, 25], however, is computationally very efficient. Both of these methods may be used to generate approximate pseudo-turbulent velocity fields.

Exact digital simulation of instantaneous turbulent flow field is also possible. McLaughlin [20] and Ounis, Ahmadi and McLaughlin [22] used the so-called direct simulation procedure for generating the instantaneous turbulent flow field in a channel for analyzing particle deposition process. This approach uses a psuedo-spectral code for solving the Navier-Stokes equation directly on a large number of grid points. The direct simulation of turbulence has become an important research tool for understanding the features of coherent structures of turbulent flows. While the method is exact and leads to an accurate description of the instantaneous flow field, it is computationally too demanding for practical applications at the present time. With the present generation of supercomputers, applications of this procedure have been limited to simulations of low Reynolds number turbulent flows in simple plane geometries. The details of the computational procedure may be found in [20, 22].

BROWNIAN MOTION

For submicron particles, the effect of Brownian motion becomes significant. To include such effects in the simulation, the Brownian force $n_i(t)$ is modeled as a Gaussian white noise random process [21-25, 46-49] with spectral intensity S_{ij}^n given by

$$S_{ij}^n = S_o\delta_{ij}, \tag{27}$$

where

$$S_o = \frac{216\nu kT}{\pi^2 \rho d^5 S^2 C_c}. \quad (28)$$

Here, T is the absolute temperature of fluid, $k = 1.38 \times 10^{-23} J/K$ is the Boltzmann constant. Amplitudes of the Brownian force components at every time step are then evaluated from

$$n_i(t) = G_i \sqrt{\frac{\pi S_o}{\Delta t}}, \quad (29)$$

where G_i is zero-mean, unit variance independent Gaussian random numbers and Δt is the time step used in the simulation. The accuracy of the simulation procedure for Brownian motion was verified by Li and Ahmadi [26] and Ounis et al. [21]. They studied several examples of diffusion of submicrometer particles from point sources. It was shown that the simulation results for ensembles of five hundred particle trajectories are in good agreement with the exact solutions for diffusion in uniform flows.

An alternative procedure for simulation of Brownian motion were described by Gupta and Peters [48]. Their method is based on the solution of the corresponding Fokker-Planck equation for a small time step. In the present method, however, the Brownian force is directly simulated as a white noise process and is added to the equation of motion of the particle. As a result, it is somewhat simpler than the technique of [48] and it is more flexible in that the coupling effects with other forces could be easily accounted for.

SIMULATION RESULTS

Dispersion and deposition of particles from point sources and from initially uniform concentrations of aerosols in an air duct were studied by Li and Ahmadi [26-29] and by Abuzeid et al. [24, 25]. In this section, a summary of the simulation results of [26-29] is presented and some additional results are discussed. For air under normal conditions, a mean velocity of $V = 5.0\,\mathrm{m/s}$ in a 2 cm wide channel was considered. Thus, the flow Reynolds number based on the channel width was about 6660. Under these flow conditions, the friction velocity is about 0.3 m/s and one wall unit of length (ν/u^*) is about 50 μm. The corresponding wall unit of time (ν/u^{*2}) is 1.67×10^{-4} s. In this case, the half width of the channel is about 200 wall units. A density ratio of $S = 2000$ and different particle diameters ranging from 0.01μm to 10μm are used in these simulations. Ensembles of three thousand samples were employed for evaluating various particle trajectory statistics and wall deposition velocities.

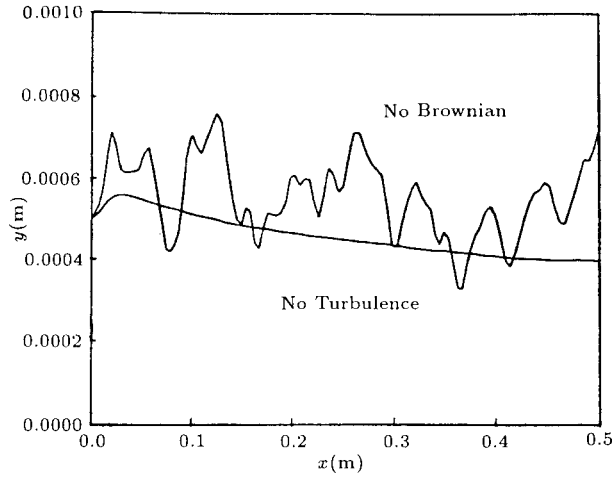

Figure 1. Sample trajectories for 1.0μm particles.

Point Source Simulation Results

Sample particle trajectories for 1μm particles are shown in Figure 1. In one case the effect of turbulence is neglected and in the other case the effect of Brownian diffusion is ignored. It is observed that the effect of turbulent dispersion is far more significant than that of molecular diffusion at distances of the order of 0.5 mm away from the wall.

Figures 2 and 3 display variations of trajectory statistics for 0.05μm and 5μm particles emanating from point sources at a distance of 10 wall units (0.50 mm) from the wall, respectively, in laminar and turbulent flows. The channel is horizontal and the gravitational force which is perpendicular to the flow direction is included

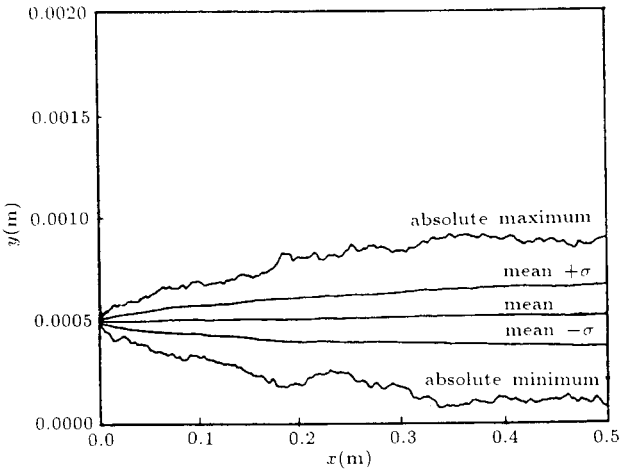

Figure 2. Trajectory statistics for 0.05 μ m particles in a laminar flow.

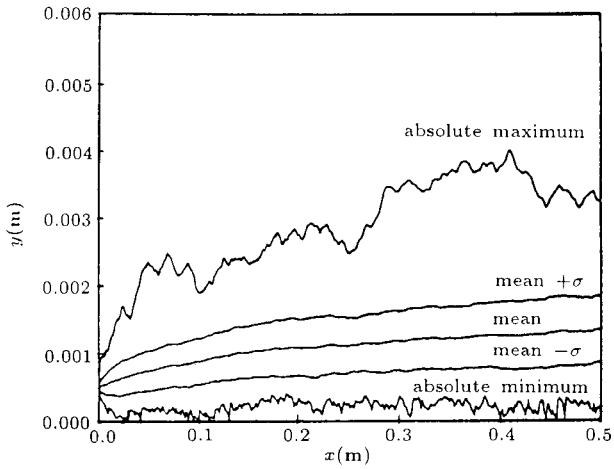

Figure 3. Trajectory statistics for 5 μ m particles in a turbulent flow.

in these simulations. Ensembles of two hundred samples were used in these studies. The dispersion of particles due to Brownian and turbulent diffusion is clearly observed from these figures. Figures 2 and 3 clearly show that the turbulent dispersion effects dominate the Brownian diffusion even at distances very near the wall.

Li and Ahmadi [26] studied the trajectory statistics of particles which are released from a point source at a distance of 1 wall unit from the wall. Their results showed that the particle spreading rates differ significantly from one another in this case. The reason for these widely different dispersion behaviors may be explained as follows. Very near the wall, the turbulent fluctuation dies down and the Brownian motion becomes the dominant mechanism for diffusion of particles less than 0.1μ m. The Brownian effect for particles larger than 0.5μ m is negligibly small. Thus, large particles which are trapped near the wall can not diffuse to the wall. The larger ones ($d \simeq 5\mu$ m) will deposit rapidly on the wall due to gravitational sedimentation. Aerosols of the order of 0.5 to 1μ m will remain suspended for a relatively long duration of time without being deposited on the surface due to the absence of significant dispersing mechanisms.

The particle trajectory statistics in a vertical channel flow where the effect of gravity is negligible was also studied in [26]. Their results showed that the trajectory statistics for 0.01μ m and 1μ m particles were not affected by the presence or the absence of gravity. For 5μ m or larger particles, however, the gravitational sedimentation significantly alters the trajectory statistics. For example, none of the 5μ m particles released from a point source at a distance of one wall unit from the wall were deposited when the gravitation field was absent.

Uniform Concentration Simulation Results

To generate a uniform concentration, the initial locations of particles were selected at random within 30 wall units. The particle initial velocity was set equal to the local fluid velocity. In [27], it was shown that simulation results for deposition rate for an initially uniform concentration within 30 wall units are in excellent agreement with those obtained for the uniform concentration across the entire channel. That is, almost all the deposited particles originated from an initial location within 30 wall units for the time duration of simulation (about 400 wall units of time). Thus, limiting the simulation region to 30 wall units leads to considerable economy of needed computational time with no loss of accuracy. The cases of vertical and horizontal channels were studied in [27]. Here the case of a vertical duct is described.

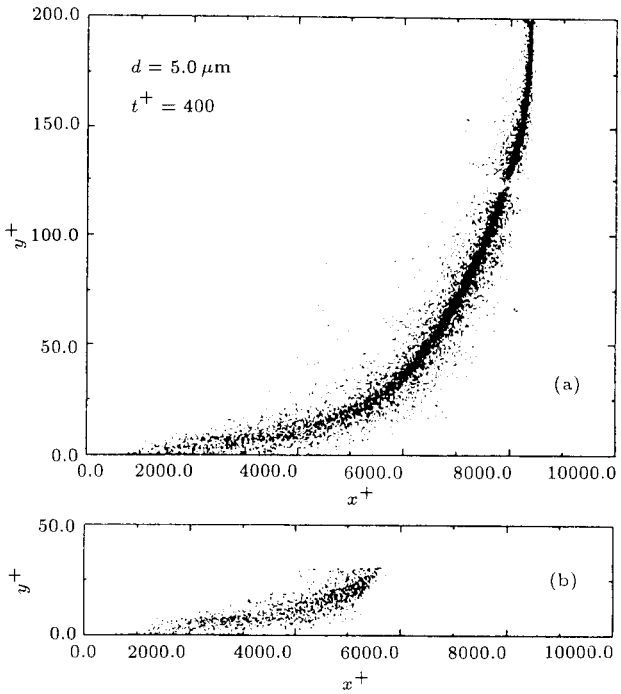

Figure 4. Distribution of 5 μm particles within the channel at $t^+ = 400$. (a) half channel simulation, (b) 30 wall units simulation.

Figure 4 shows the distribution of 25,000 particles which are released uniformly at the inlet of the vertical channel. It is observed that the particles are being transported by the mean velocity field and being dispersed by turbulence fluctuations. The corresponding concentration field is shown in Figure 5. It is observed that the concentration of 5 μm particles has a rather sharp peak near the wall. The reason is that the particles are being moved toward the wall by the turbulence fluctuations. However, very close to the wall, the turbulence intensity becomes negligible. Furthermore, the Brownian diffusion of these relatively large particles is also too small to make them deposit on the wall. Migration of particles to regions with lower turbulence intensity is refered to as the turbophoresis phenomenon [50].

For a uniform particle concentration C_o near a surface, the deposition velocity is defined as

$$u_d = J/C_o, \tag{30}$$

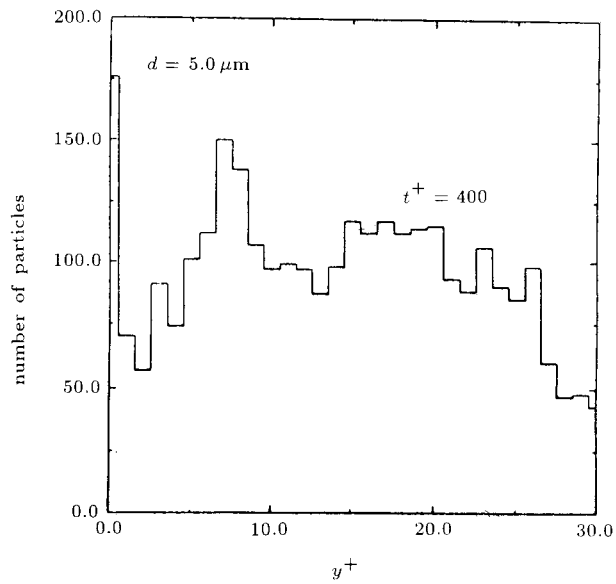

Figure 5. Concentration of 5 μm particles near the wall in a vertical channel.

where J is the particle flux to the wall per unit time. The nondimensional deposition velocity given as

$$u_d^+ = u_d/u^*, \tag{31}$$

is commonly used in the literature as a convenient measure of particle flux to the wall. In simulation studies, when an initial number of particles N_o are uniformly distributed in a region within the distance of H_o^+ from the wall, the nondimensional deposition velocity is given by

$$u_d^+ = \frac{N_d/t_d^+}{N_o/H_o^+}, \tag{32}$$

where N_d is the number of deposited particles in the time duration t_d^+. In practice, t_d^+ should be selected in the quasi-equilibrium condition when N_d/t_d becomes a constant.

Figure 6 shows variation of nondimensional deposition velocity with nondimensional particle relaxation time defined as

$$\tau^+ = \frac{Sd^2u^{*2}}{18\nu^2}C_c. \tag{33}$$

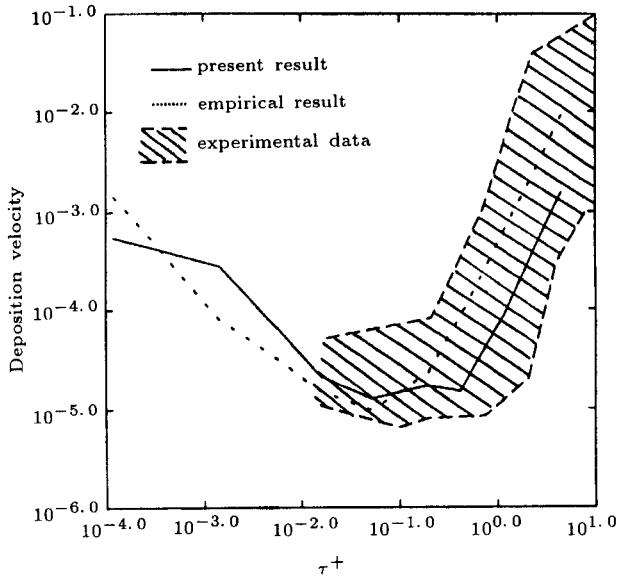

Figure 6. Variation of particle deposition velocity with nondimensional particle relaxation time for a vertical channel.

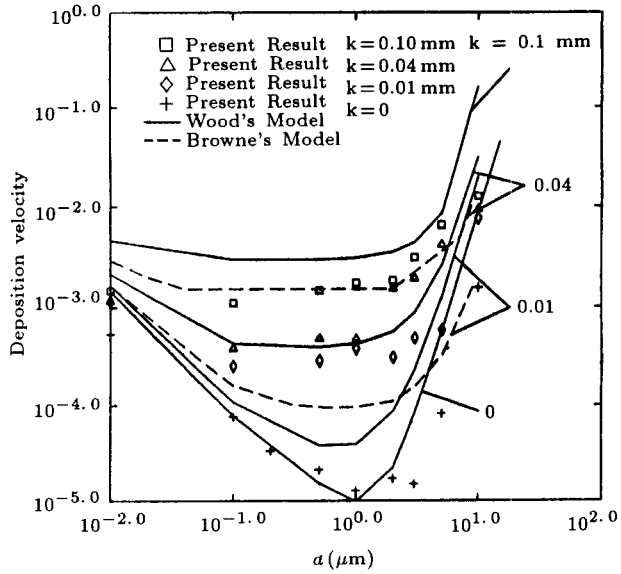

Figure 7. Variation of particle deposition velocity with particle diameter for a vertical channel.

In this figure, the solid line is the present simulation results, and the dotted line is result calculated from the empirical equation suggested by Wood [11] given as

$$u_d^+ = 0.57Sc^{-\frac{2}{3}} + 4.5 \times 10^{-4}\tau^{+2}, \qquad (34)$$

where Sc is the Schmidt Number defined as

$$Sc = \nu/D, \qquad (35)$$

with D being the particle mass diffusivity. The experimental data as collected by Papavergos and Hedley [14] are also shown in this figure for comparison. It is observed that the simulation results are in agreement with the experimental data. The present result is also in qualitative agreement with the empirical equation given by Equation 34 in trend of variations. However, compared with the empirical one, the present simulated deposition velocities are somewhat lower for $\tau^+ > 0.1$.

Rough Wall Simulation Results

Deposition of particles on rough walls from an initially uniform concentration of aerosols in a 2 cm wide channel was studied by Li and Ahmadi [28]. Ensembles of three thousand samples were employed for evaluating various particle trajectory statistics and wall deposition velocities.

Figure 7 shows variation of nondimensional deposition velocity with particle diameters. In this figure the dashed lines and solid lines are results, respectively, from Browne [10] and Wood [11]. It is observed that the simulation results are in qualitative agreement with the empirical equations, but there are quantitative differences. For a roughness of 0.04 mm, the simulation results are in the range of the theoretical predictions of [10] and [11]. However, the simulation results are higher for a roughness of 0.01 mm and somewhat lower for a roughness of 0.1 mm when compared with those of the theoretical models.

Figure 7 shows that the increase of wall roughness increases the number of deposited particles. This is because the turbulent intensity increases as the roughness increases. Furthermore, the increase of roughness increases the particle capture distance from the wall. The turbulent fluctuation also remains finite at the tip of the roughnesses. These cause the turbulent dispersion effect to be more effective. Therefore, the increase of roughness makes the turbulent

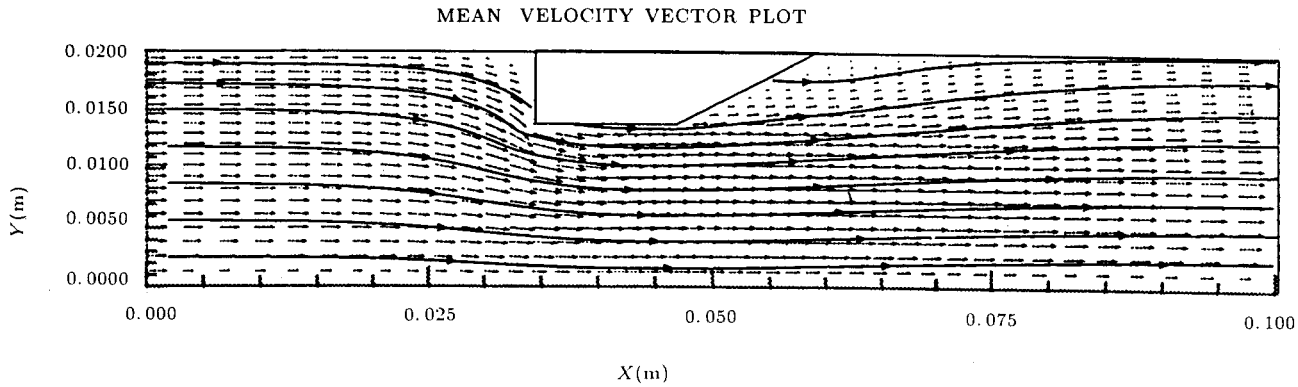

Figure 8. Mean velocity vector plot and streamlines in the duct.

eddy impaction process to become the dominant mechanism of deposition even for smaller particles. As a result, the deposition velocity remains approximately constant at high roughness for small particles.

Complex Geometry Passages

The STARPIC-RATE computational code was used by Li et al. [29] for simulating the mean turbulent flow conditions and particle transport and deposition in a duct with obstructing blocks of various shapes. In these computations, it was assumed that the mean flow is steady and a staggered grid with 24×46 node points was used. Uniform profiles for the mean velocities, turbulence kinetic energy and dissipation rate were specified at the inlet. For the grids near the wall, the standard wall function boundary conditions were used. At the outlet, zero normal gradient conditions were specified. Ensembles of one-thousand samples were employed for evaluating various particle trajectory statistics and wall deposition rates.

Figures 8-10 show the mean velocity vector plot, the turbulent kinetic energy, the dissipation rate, and the streamwise and vertical root-mean-square fluctuation intensities e_1 and e_2. It is observed that a large recirculation region behind the block is formed. The air flow also accelerates in the region in front and along side of the block. Near the tip of the block and in the recirculation region a high level of turbulent fluctuation is observed. The energy dissipation rate is also very high near the front corner of the block as well as in the recirculation zone. Figure 10 also clearly shows that the turbulence is anisotropic. In the recirculation region, the root-mean-square streamwise fluctuation e_1 component is much larger than the vertical components e_2.

Figure 11 displays variations of particle trajectory statistics for different diameters from a point source at a distance of 0.2 cm from the upper wall ($Y_o = 0.018$ m). The gravitational effect is neglected in these simulations. The mean particle paths are shown by the solid lines. Here σ corresponds to the standard deviation of particle trajectories in the vertical direction. The absolute maximum and minimum trajectories for an ensemble of 1000 particles are also shown in this figure for reference. While these are sample dependent, they provide additional information on the spreading of particles. The numbers listed on various surfaces in this figure denote the number of deposited particles. For 10 μm particles, it is observed that 995 particles are deposited on the front surface of the block and only five particles leave the duct. For 1 μm and 0.01 μm particles, respectively, 143 and 133 particles reach the front surface of the block. In addition, five 1 μm particles and three 0.01 μm particles deposit on the surface of the upper wall behind the block. The high deposition rate of 10 μm particles shows that the inertia impaction mechanism is quite effective for these relatively large particles. The 0.01 μm particles

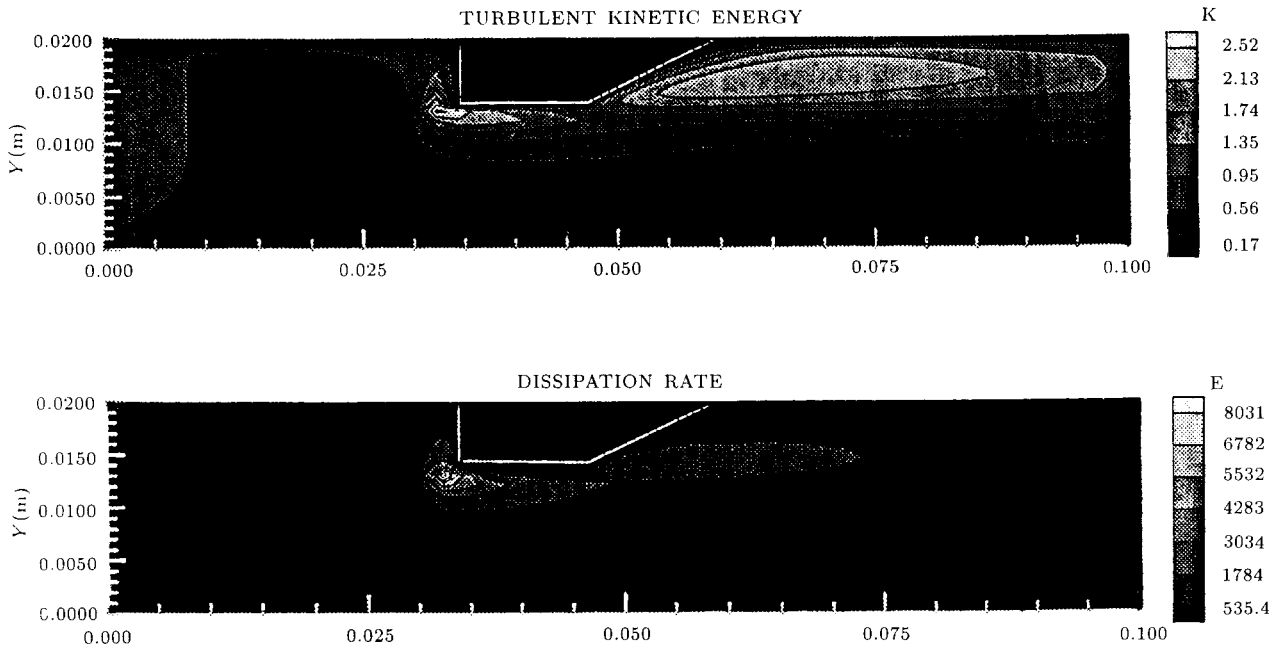

Figure 9. Turbulence kinetic energy and dissipation rate distribution in the duct.

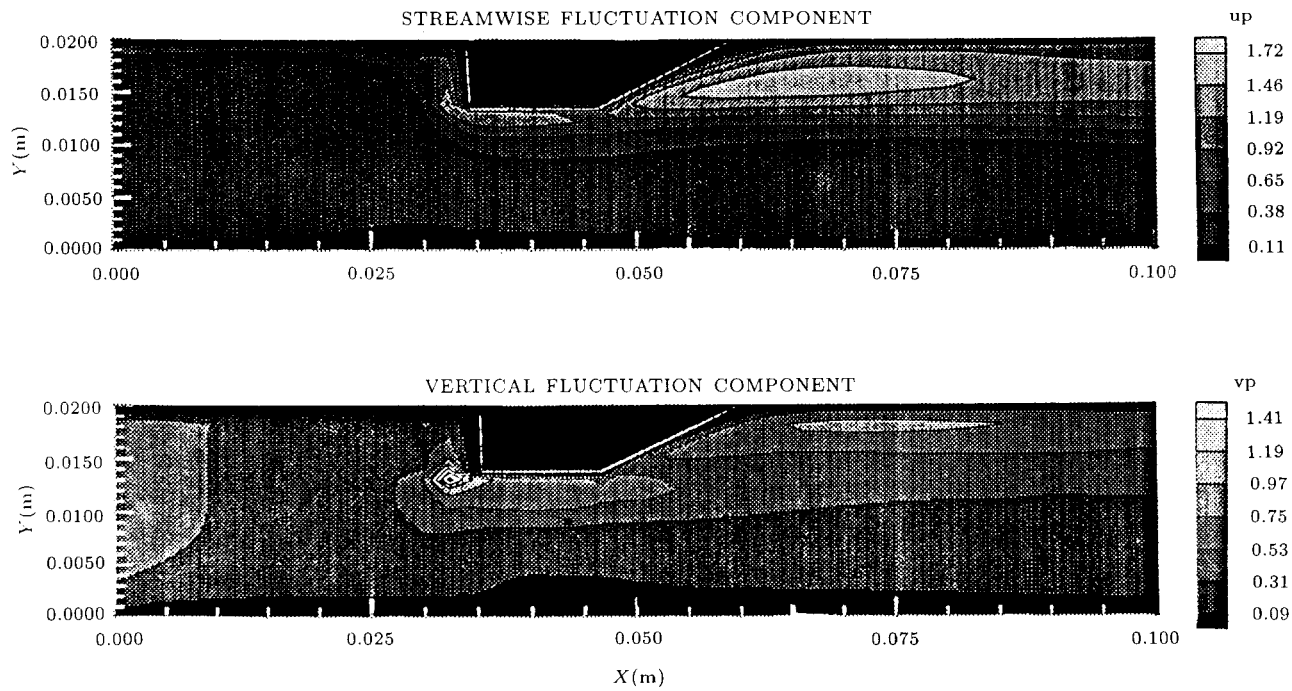

Figure 10. Distribution of turbulence fluctuation energy components in the duct.

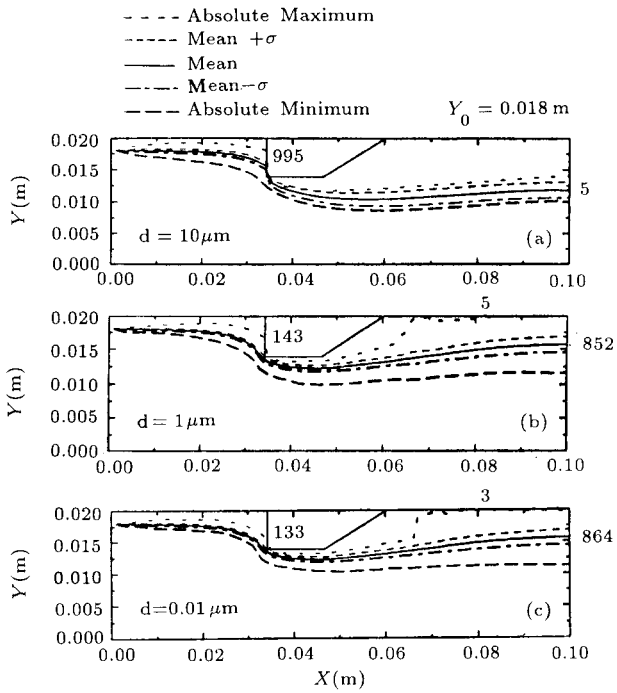

Figure 11. Particle trajectory statistics for different diameters: (a) $d = 10\,\mu$m, (b) $d = 1\,\mu$m, (c) $d = 0.01\,\mu$m.

are, however, deposited mainly due to diffusion.

Direct Simulation Procedure

An exact simulation procedure for simulating the instantaneous turbulent velocity field in the channel for analyzing deposition of submicron particles was used by Ounis, Ahmadi and McLaughlin [22]. The flow field was generated by the so-called direct numerical simulation of the Navier-Stokes equation. It was assumed that the flow is driven by a constant mean pressure gradient. Based on the hydraulic diameter of the channel and the mean velocity, the Reynolds number was approximately 6500. Instantaneous flow patterns generated in [22] showed the presence of rather persistant coherent vortices in yz-plane. In particular, strong flow streams towards the wall and away from it due to the formation of counter rotating vortices were clearly observed.

One of the studies performed by Ounis et al. was to determine the distributions of

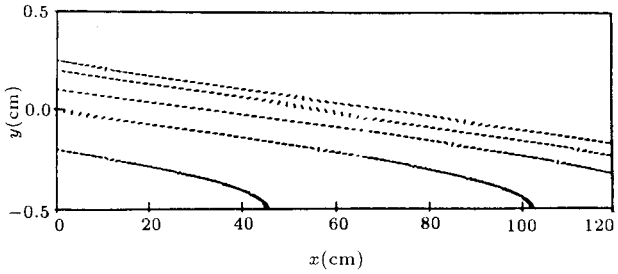

Figure 12. Sample trajectories of ellipsoidal particles in a Poiseuille flow.

the initial locations of the deposited particles of different sizes. They found that the initial locations of deposited 0.05 and 0.1 μm particles were concentrated on relatively narrow bands along the channel. The spacing between these bands were of the order of 100 to 150 wall units which is consistent with the available estimates for the distance between streaks in a turbulent boundary layer near a wall [44]. This result clearly showed that near wall coherent vortices strongly affect the particle deposition process.

Ellipsoidal Particles

In this section, certain simulation results concerning dispersion and wall deposition of nonspherical particles are presented. Elongated particles are strongly affected by the flow shear field, and the translational and rotational Brownian motions. As a result of the shear, these particles tend to orient themselves along the flow direction. The Brownian effect, however, tends to randomize the particle orientation. Depending on size and aspect ratio of particles, and the strength of the shear rate one of the two effects could become dominant.

Figure 12 shows sample trajectories of elongated particles undergoing gravitational sedimentation in a laminar Poiseuille flow in a horizontal channel. The particles are ellipsoids of revolution with the semi-minor axes of $a = 0.5\,\mu$m and the aspect ratios of $\beta = 15$. The velocity field is given as, $u = u_o[1 - (y/h)^2]$, with an averaged flow velocity of 5.7 cm/sec. The Brownian motion is neglected in these simulations.

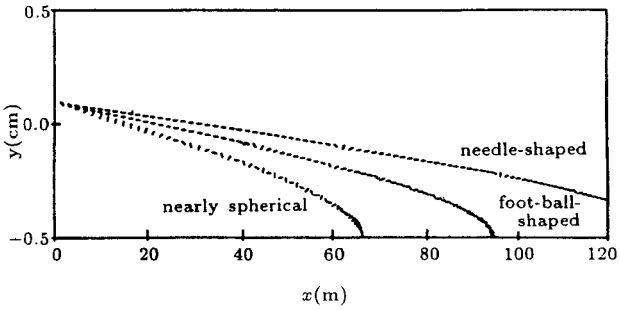

Figure 13. Sample trajectories and orientation of elongated particles of different aspect ratios.

The particles are released from various locations across the channel with their major axes being either parallel or perpendicular to the flow direction. It is observed that, as the particles are transported downstream, they sediment and rotate due to the actions of gravity and velocity gradient. The rotational motions of particles are related to the local fluid vorticity. Thus, the particles rotate counter-clockwise in the upper half of the channel, while their rotation is clockwise in the lower half of the channel. It is also observed that the particles tend to orient themselves so that their major axes remain parallel to the flow direction.

Figure 13 displays the trajectories and orientation of particles with different shapes in a Poiseuille flow during gravitational sedimentation. Three particles being considered are a highly-elongated needle-shaped particle, a foot-ball-shaped ellipsoidal particle, and a nearly-spherical particle. All of the three particles are volumetrically equivalent to an ellipsoid of revolution with the major axis of $15\,\mu$m and the minor axis of $1\,\mu$m. The particles are released initially with their major axes perpendicular to the flow direction. It is noticed that the needle-shaped particle travels the longest distance and essentially remains oriented with the flow direction. As the aspect ratio decreases, the time duration that the particle maintains its orientation reduces and the particle flight distance decreases.

Figure 14 shows the motion of an ellipsoidal particle in a laminar plane stagnation-point flow. The particle is initially released from $x = 8.5 \times 10^{-7}$ m and $y = 1.278 \times 10^{-3}$ m with its major axis being perpendicular to the wall. It is observed that the particle is transported downward by the incoming flow and rotates in the vicinity of the wall due to the flow shear in the boundary layer. It is also noticed that the particle is eventually intercepted by the wall at $x \simeq 1.278 \times 10^{-3}$ m.

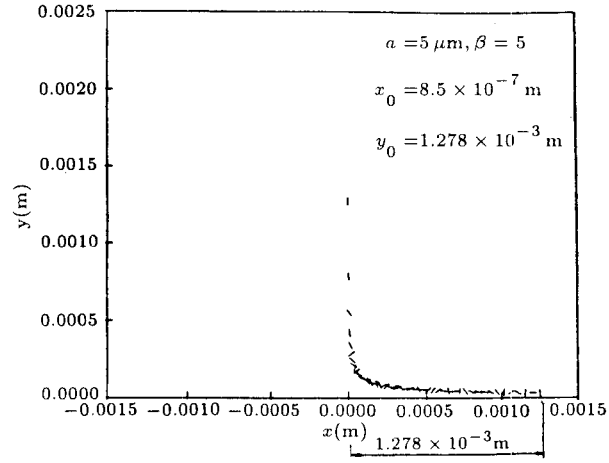

Figure 14. Limiting trajectory of an ellipsoidal particle in a stagnation point flow.

Figure 15 shows trajectories and orientations of ellipsoidal particles in a laminar simple shear flows with, $u = (u_o + \dot{\gamma}y)\hat{i}$. Here, $u_o = 3.7\,$cm/s and different shear rates ($\dot{\gamma}$) are used. The semi-minor axes and the aspect ratios of the particles are $a = 0.414\,\mu$m and $\beta = 10$,

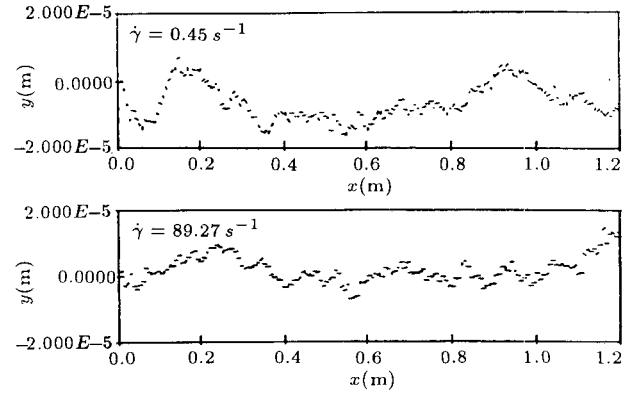

Figure 15. Trajectories and orientations of ellipsoidal particles with $a = 0.414\,\mu$m and $\beta = 10$ in simple shear flows with $u_o = 3.7\,$cm/s and different shear rates.

respectively. The particle equation of motion used includes both translational and rotational Brownian motion effects. The particles are released initially from the origin with their major axes parallel to the flow direction. It is observed that, for small shear rate, the orientation of the ellipsoidal particle is quite random and the particle trajectory has an almost totally random pattern. The translational Brownian motion causes the particle to follow a random pattern as it is transported downstream, while the rotational Brownian motion randomizes the particle orientation. For large shear rate, however, the ellipsoidal particle remains oriented with its major axis parallel to the flow direction for a long duration of time. As noted before, the orientation of nonspherical particles in shear flows is the result of two competing processes. The Brownian effect tends to randomize the particle orientation while the flow shear tends to orient the particle. A sufficiently high shear rate overcomes the Brownian motion and orients the elongated particle along the flow direction.

Figure 15 shows that the particle displacement in the y-direction for the small shear rate condition is larger than that for the large shear rate condition. This is due to the smaller lateral mobility of the elongated particle when it is oriented parallel to the flow direction.

Figure 16 shows the diffusion and deposition of ellipsoidal particles of different sizes from a point source in a laminar simple shear flow. The particles are ellipsoids of revolution with aspect ratios of $\beta = 10$, and are initially released from the point source located at $x^+ = 0.0$ and $y^+ = 0.2$. The statistics are obtained from an ensemble of 50 particle trajectories. It is observed that, as the particles are being transported downstream, they are dispersed laterally due to the effect of Brownian motion. A comparison of the diffusion patterns for different-size particles shows that the Brownian diffusion is more significant for small-size particles. For $a^+ = 0.011$, the diffusion pattern is roughly symmetric with respect to the mean trajectory, and no particle deposition is observed. As a^+ decreases to 0.00055, however, the particle dispersion rate increases considerably. Figure 16 shows that several particles also deposit on the wall. The diffusion pattern in this case is no longer symmetric due to the deposition of particles.

The Brownian diffusions of ellipsoidal particles from different initial distributions in a simple shear flow are shown in Figure 17. Various statistics are obtained from ensembles of 100 particle trajectories. It is observed that the Brownian motion causes the particles to spread laterally as they are transported downstream by the flow. Figure 17 also shows the diffusion

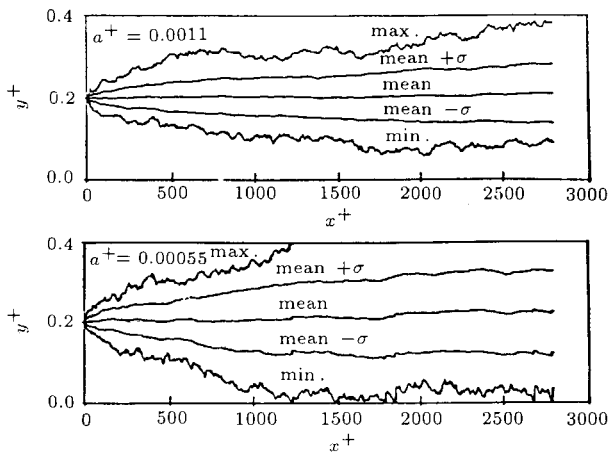

Figure 16. Diffusion of ellipsoidal particles with $\beta = 10$ from a point source in a simple shear flow.

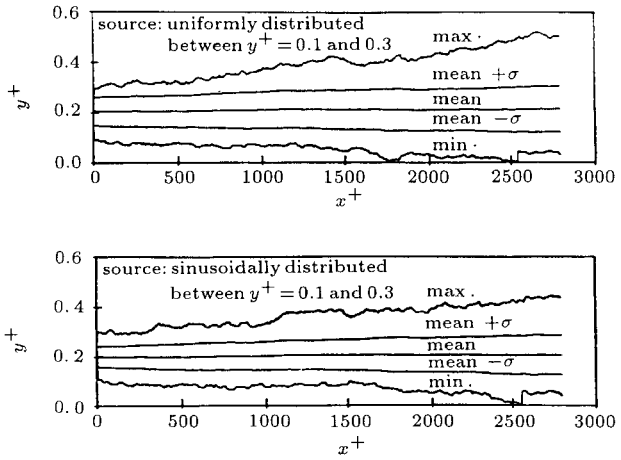

Figure 17. Diffusion of ellipsoidal particles with $a^+ = 0.0011$, $\beta = 10$ from sources with various distributions in a simple shear flow.

patterns are similar for the two different initial particles distributions considered.

SUBLAYER MODEL

It is well known that the turbulent near wall flow is a region of strong dynamic interactions where most of the turbulence fluctuation energy is generated. From numerous flow visualization experiments and direct numerical simulations, it is now well recognized that the turbulent near-wall region is dominated by coherent vortical structures and roughly cyclic busting phenomena. Hinze [44] provided a description for the general features of formation of coherent vortices and down sweep and busting processes. Accordingly, the spacing between the streaks are about 100 wall units ($\Lambda^+ \simeq 100$). These near-wall vortex structures are believed to be responsible for turbulent deposition of small particles. The simulation results of Ounis, Ahmadi and McLaughlin [22] also clearly showed that the down sweep flow generated by these persisting coherent vortices are the main mechanism that carries the particles to the wall. Since the up-flow regions do not contribute to particle deposition, only the flow pattern toward the wall need to be modeled.

Along the line of [8, 9], Fan and Ahmadi [30] developed a model for predicting the particle deposition rate in turbulent flows. It was assumed that the down sweep flow pattern generated by the coherent wall vortices may be approximated by a steady two-dimensional viscous stagnation point flow. The observed prolonged persistence of streamwise coherent vortices justifies the assumption of steady flow condition. Additional results concerning the model predictions of [30] are described in this section.

Figures 18 and 19 show variations of the nondimensional deposition velocity, u_d^+, for particle-to-air density ratios of 1500 and 500 and different flow Reynolds number with the dimensionless particle relaxation time. In these figures, the collected experimental data are shown by solid dots. The solid lines correspond to the

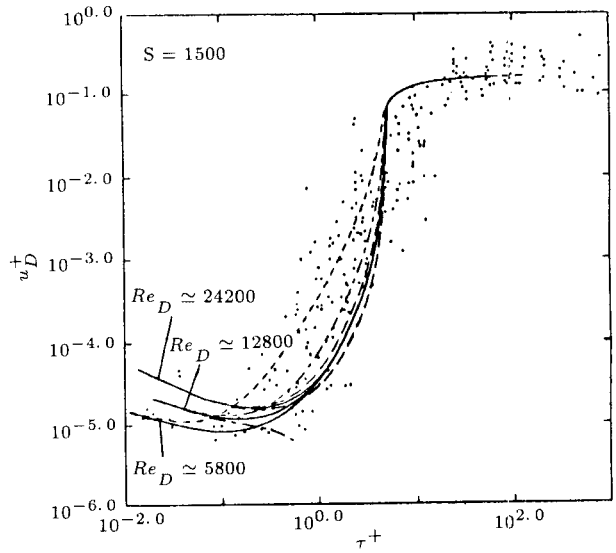

Figure 18. Variation of deposition velocity with nondimensional particle relaxation time for a vertical channel.

sublayer model predictions for $g^+ = 0$. There are two dashed lines accompanying each solid line in Figure 18 and 19.The one above the solid line corresponds to the system in which the flow is in the direction of gravity, while the one below the solid line is for the system in which the flow direction is opposing gravity. It is observed that the increasing trend of the inertia dominated particle deposition rate with τ^+ is well predicted by the model. Comparing the predicted results with those obtained from experiments shows that the model provides reasonable estimates for deposition velocities. It is observed that the inertial-controlled deposition as predicted by the present model is independent of flow Reynolds number while the diffusion-controlled deposition increases as Re_D increases.

Comparing Figures 18 and 19 shows that the deposition velocities for $\tau^+ > 0.1$ decrease as the density ratio increases, while those for submicron particles increase with an increase in density ratio. This is because particles with larger density ratios correspond to smaller sizes for a given τ^+. The interception capturing process by the surface is less efficient for smaller particles which causes the intertial-controlled deposition to decrease. On the other hand, the

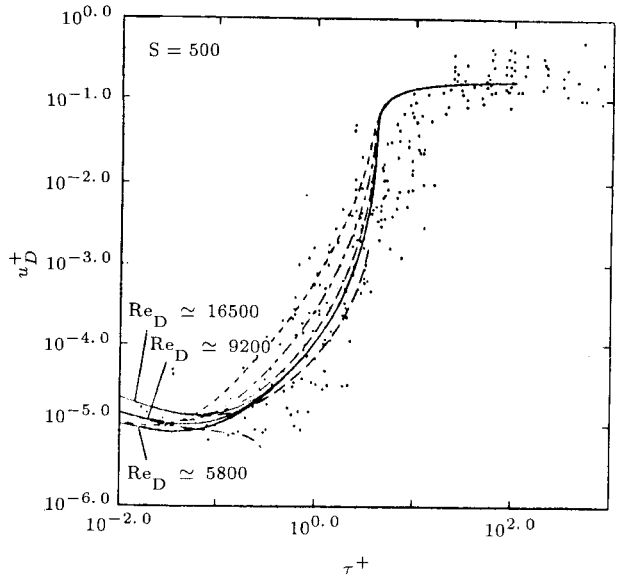

Figure 19. Variation of deposition velocity with nondimensional particle relaxation time for a vertical channel.

Brownian motion is more significant for smaller particle which lead to the increase of diffusion-controlled deposition rate.

The flow direction also affects the deposition velocities in a vertical pipe through the shear-induced lift force. Figures 18 and 19 show the effects of flow direction on the deposition velocity for various flow Reynolds numbers and different density ratios. It is observed that the particle deposition in a vertical channel is enhanced when the flow is in the direction of gravity and is reduced when the flow is opposing gravity. The magnitude of the deviation depends on the flow Reynolds number. The variation of deposition velocities with flow direction is more significant for flows with lower Reynolds numbers. Variations of the deposition velocity with density ratio and flow direction may provide an explanation for the observed scatter of the experimental data.

From Figures 18 and 19, it is also noticed that some dashed lines for the system with flow opposing gravity do not cover the entire range of τ^+ considered. This is because the shear-induced lift force in the system tends to reduce the particle deposition rate. As the particle size increases, the magnitude of the lift force also increases to the level that eventually prevents the particle from being deposited. It should be pointed out, however, that the averaged streamwise velocity was used in the model of [30]. In turbulent flows, the streamwise velocity field fluctuates randomly due to the bursting process. That could allow for a small amount of particle deposition at certain periods of time. However, this latter effect was neglected in this study.

A semi-empirical equation for calculating the inertial-controlled deposition rate in a vertical channel was proposed in [30]. For a duct with smooth wall, the corresponding equation is given by,

$$u_{di}^+ = \frac{\Lambda^+}{4}\left[\frac{\frac{d^{+2}}{4} + \frac{\tau^{+2} g^+ L_1^+}{\beta(1+\tau^{+2}L_1^+)}}{(1.85)^2 + \frac{\tau^{+2} g^+ L_1^+}{\beta(1+\tau^{+2}L_1^+)}}\right]^{\frac{1}{1+\tau^{+2}L_1^+}} \left[1 + 8e^{-(\tau^+-10)^2/32}\right] \frac{(1.85)^2\beta}{1 - \tau^{+2}L_1^+(1 + \frac{g^+}{(1.85)^2\beta})}, \tag{36}$$

where $\beta = 0.01085$ is a constant and L_1 is the nondimensional lift parameter given by

$$L_1 = 3.08/(Sd^+), \tag{37}$$

Equation 36 indicates that the inertial-controlled deposition rate depends on the density ratio, the flow direction, and the flow Reynolds number. Effects of the flow direction appears to have been ignored in the current literature.

Figure 20 shows the variations of deposition velocity for various flow Reynolds numbers with the particle relaxation time as predicted by the empirical Equation 36. The solid line shown in this figure is accompanied by two dashed lines. The one above the solid line corresponds

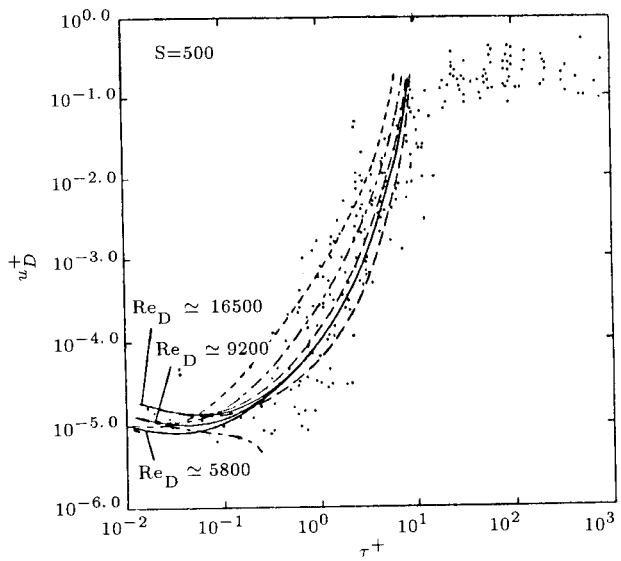

Figure 20. Variation of deposition velocity with particle relaxation time as predicted by the empirical equation.

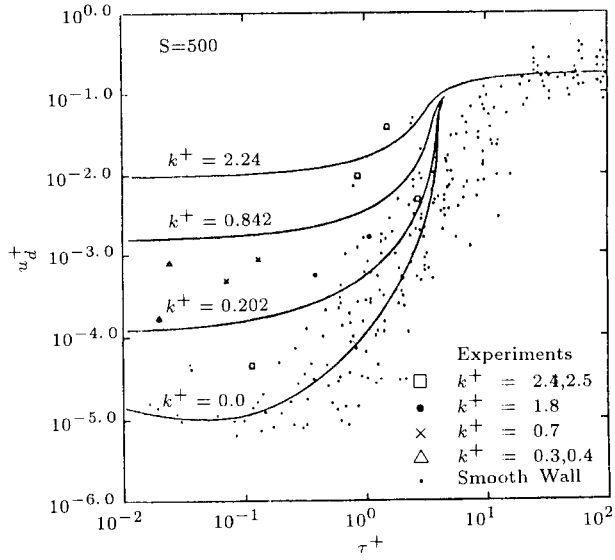

Figure 21. Variation of particle deposition velocity with particle relaxation time and wall roughness.

to the system with flow in the direction of gravity, while the one below the solid line is for the system with flow opposing gravity. It is observed that the empirical equation provides reasonable predictions for the deposition velocity. Furthermore, a comparison of Figure 20 with Figure 19 shows that the proposed empirical equation retains the general features of the effects of flow direction and the flow Reynolds number on the predicted deposition velocities.

A Model for Rough-Wall Deposition

The sublayer model for turbulent deposition was extended to rough vertical walls by Fan and Ahmadi [30]. The model predictions for the deposition velocities other than those used in [30] are presented here. The results are compared with the limited available experimental data. The effects of wall roughness and the flow direction on the deposition rate are also discussed.

Figure 21 shows the variations of nondimensional deposition velocity with the dimensionless particle relaxation time for a density ratio of $S = 500$ and for various wall roughnesses. The gravitational effect is neglected for the results presented in this figure. Here, k^+ is the averaged height of the surface roughness in wall units. It is observed that, for a small roughness, the deposition rate is very sensitive to the variations of particle relaxation time. As τ^+ increases, the deposition velocity first decreases to a minimum value at $\tau^+ \simeq 0.1$. Beyond this value of τ^+, the deposition velocity increases rapidly with τ^+ up to τ^+ of about 10. For $\tau^+ > 10$, the deposition velocity remains almost constant with $u_d^+ \simeq 0.1$. The decrease of u_d^+ with an increase in τ^+ for small particles is due to the reduction of Brownian diffusion effects. For $\tau^+ > 0.1$, the deposition is mainly controlled by the eddy-impaction process. Thus, the deposition velocity increases with an increase in τ^+.

Figure 21 also shows that the deposition rate increases significantly with wall roughness for $\tau^+ < 5$. In the rough wall conditions, the particle deposition is mainly controlled by the eddy-impaction process for the particle sizes considered. It is also observed that, as wall roughness increases, u_d^+ becomes almost independent of τ^+ for small particle relaxation times. For rough walls, experimental data for particle deposition are rather scarce. Montgomery and

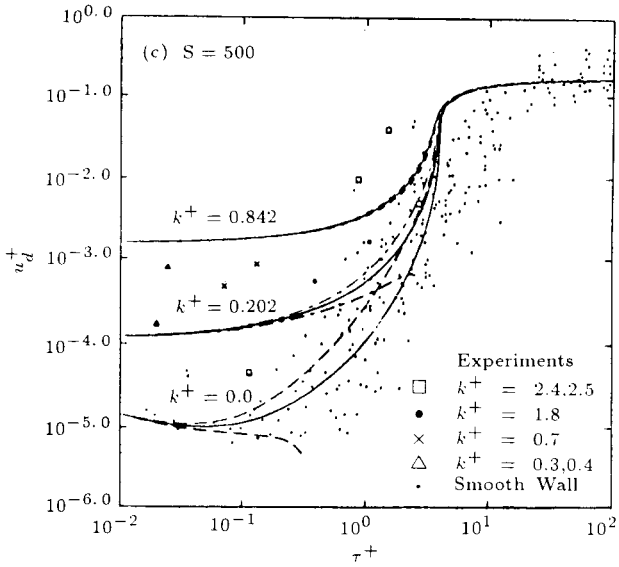

Figure 22. Variation of particle deposition velocity with particle relaxation time and wall roughness.

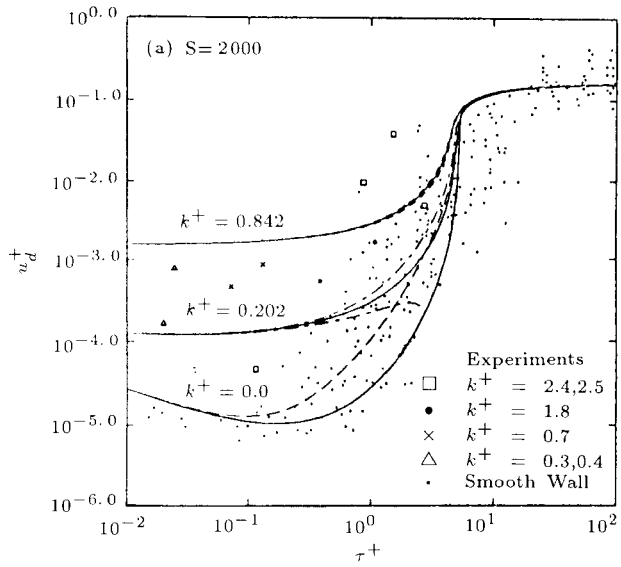

Figure 23. Variation of particle deposition velocity with particle relaxation time and wall roughness.

Corn [51] reported a limited number of experimental data. A comparision of the prediction of the model with the experimental data shows that the model provides a reasonable estimate for the deposition velocity.

The effects of flow direction on the deposition rate for spherical particles on a rough surface in a vertical channel are shown in Figures 22 and 23. Density ratio of 500 and 2000 are considered and the gravitational force and the shear-induced Saffman lift are included in the analysis. In these figures, the solid lines correspond to the cases when $g^+ = 0$. As noted before, the dashed line above the solid line corresponds to the system in which the flow is in the direction of gravity, while the one below the solid line is for the system in which the flow direction is opposing gravity. It is observed that the particle deposition rate in a vertical channel is enhanced when the flow is in the direction of gravity and is reduced when the flow is opposing gravity. Figures 22 and 23 also show that the effect of flow direction on the turbulent deposition is more significant for smooth surfaces. As the wall roughness increases, the deposition velocity becomes almost independent of the flow direction. In addition, the density ratio does not have a significant effect on the nondimensional deposition velocity.

Electrical Precipitation in a Turbulent Vertical Channel

Electrical precipitation of aerosol particles in a turbulent vertical channel was considered by Fan and Ahmadi [31]. The sublayer model was extended to include the effect of electric field on charged particles. Figure 24 shows variations of deposition velocity with particle relaxation time for $S = 965$ and various electric field strengths. It is assumed that the charged particles follow a Boltzmann distribution and the averaged number of charge for different size particles are used in the analysis, while the gravitational force is neglected. It is observed that the presence of electric field affects the deposition rate significantly for $\tau^+ < 1$. For $\tau^+ > 1$, the deposition rate is insensitive to variations of the electric field intensity.

The effects of the flow direction on deposition rate is shown in Figure 25. The three solid lines shown in the figure are for the cases when $g^+ = 0$. It is noticed that there are two dashed lines accompanying each solid line. The

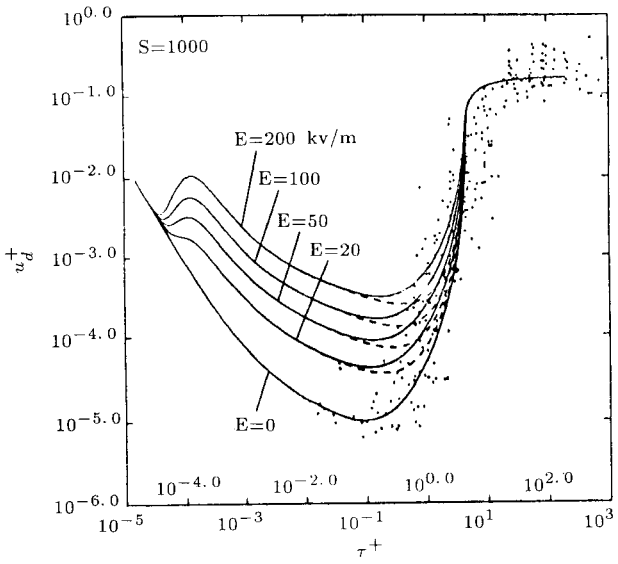

Figure 24. Variation of deposition velocity of charged particles with nondimensional particle relaxation time for different electric field intensities.

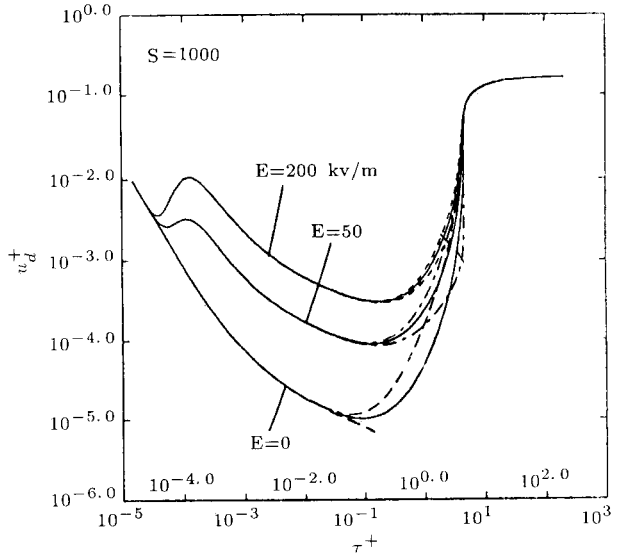

Figure 25. Effect of flow direction on deposition velocity for different electric field intensities.

one above the solid line is for the down-flow system while the one below the solid line is for the up-flow system. This figure shows that the particle deposition rate is enhanced by using a down-flow system, while it is reduced by using an up-flow system.

CONCLUSIONS

In this work, the recently developed digital simulation methodology for studying deposition of aerosol particles on surfaces in turbulent flow is described. The STARPIC-RATE computational model for evaluating the mean velocity profile and the components of the root-mean-square turbulent intensities is outlined. The procedures for simulating the instantaneous turbulence fluctuation field as a continuous Gaussian random process is outlined. The direct simulation of the instantaneous turbulent velocity field is also discussed. The particle equation of motion which includes the fluid drag, the Brownian force, the Saffman lift force and the electrostatic force is described. Sample simulation results are presented and ensembles of trajectories for particles of different sizes are generated and statistically analyzed. The cases of horizontal and vertical duct as well as the flow in an air passage with an obstructing block are analyzed. Simulation results concerning the effects of various forces on dispersion and deposition of spherical particles are presented. The effects of nonsphericity of particles are also discussed. A sublayer model, which is based on the coherent vortical structure of near wall turbulence, for deposition øf particles from turbulent air streams on smooth and rough surfaces in a vertical duct, is also presented. Extensions of the model to rough surfaces and presence of electrostatic forces are also discussed.

Based on the presented results, the following conclusions may be drawn:

1. The simulation methodology provides a powerful tool for studying particle dispersion and wall deposition processes in turbulent air flows in clean rooms and process equipment.
2. Digital simulation results are in good agreement with the experimental data and the empirical equations.
3. Variation of deposition rate of particles with size follows a V-shape curve.

4 For large particles, the deposition rate increases rapidly with particle size.

5. Brownian force significantly affects the dispersion of small aerosol particles within the inner region of viscous sublayer of about 1 wall unit from the surface.

6. Small particle deposition rate increases rapidly with a decrease in particle diameter.

7. Except for the region very near the wall, turbulence is the dominating dispersing mechanism.

8. Gravitational effect significantly increases the deposition velocity for particles larger than 2μ m.

9. In the vertical channel, the minimum deposition rate occurs for particle diameters in the range of $0.5 - 3.0\mu$ m. For the horizontal channel, the gravitational effect shifts the position of minimum to $0.1 - 0.3\mu$ m size range.

10. Increase of wall roughness increases particle deposition velocity.

11. The V-shape variation of the deposition velocity with particle relaxation time (and/or diameter) smooths out as wall roughness increases.

12. At high roughnesses, the deposition velocity becomes independent of diameter for particles smaller than 2μ m.

13. The direct simulation results show that the initial location of deposited particles are concentrated in the bands where the coherent vortices form strong streams towards the channel wall.

14. The proposed sublayer model provides reasonable estimates for the deposition velocity.

15. The sublayer model shows that for the inertial controlled regimes, $1 < \tau^+ < 10$, the deposition velocity increases rapidly with τ^+

16. The model indicates that the deposition velocities of small aerosol particles depend on density ratio, flow direction, and flow Reynolds number.

17. The sublayer model shows that the shear -induced lift force and the gravitation force significantly affect the turbulent deposition rate on smooth and rough surfaces.

ACKNOWLEDGEMENTS

The author would like to thank Mr. Michael A. Gaynes and Mr. Raymond G. Bayer of IBM-Endicott, and Dr. Douglas W. Cooper of IBM-Watson Research Center for many helpful discussions. Financial support for different parts of this work, which was provided by the International Business Machines Corporation (IBM-Endicott) and the New York State Science and Technology Foundation through the Center for Advanced Material Processing (CAMP), is gratefully acknowledged.

REFERENCES

1. Cooper, D.W. "Particulate contamination and microelectronics manufacturing: An introduction," *Aerosol Sci. and Tech.*, **5**, pp 287-299 (1986).
2. Cooper, D.W. Peters, M.H. and Miller, R.J. "Predicted deposition of submicron particles due to diffusion and electrostatics in viscous axisymmetric stagnation point flow," *Aerosol Sci. and Tech.*, **11**, pp 133-142 (1989).
3. Liu, B.Y.H. and Kang-ho Ahn. "Particle deposition on semiconductor wafers," *Aerosol Sci. and Tech.*, **6**, pp 215-224 (1987).
4. Levich, V.G. *Physicochemical Hydrodynamics*, Prentice-Hall, Englewood Clifts, NJ (1972).
5. Fuchs, N. A. *The Mechanics of Aerosol*, Pergamon Press, Oxford (1964).
6. Davies, C.N., *Aerosol Science*, Academic Press, London (1966).

7. Friedlander, S.K. and Johnstone, H. H. "Deposition of suspended particles from turbulent gas stream," *Ind. Eng. Chem.*, **49**, p 1151 (1957).
8. Cleaver, J.W. and Yates, B. "A sublayer model for the deposition of particles from a turbulent flow," *Chemical Eng. Sci.*, **30**, pp 983-992 (1975).
9. Fichman, M., Gutfinger, C. and Pnueli, D. "A model for turbulent deposition of aerosol," *J. of Aerosol Sciences*, **19**, pp 123-136 (1987).
10. Browne, L.W.B. *Atmospheric Environment*, pp 801-816 (1978).
11. Wood, N.B. "A simple method for the calculation of turbulent deposition to smooth and rough surfaces," *J. of Aerosol Sciences*, **12**, pp 276-290 (1981).
12. Wood, N.B. "The mass transfer of particles and acid vapour to Cooled Surfaces," *J. Institute of Energy*, **76**, pp 76-93 (1981).
13. Hidy, G. M. *Aerosols, An Industrial and Environmental Science*, Academic Press, New York (1984).
14. Papavergos, P.G. and Hedley, A.B. "Particle deposition behavior from turbulent flow," *Chem. Eng. Des.*, **62**, pp 275-295 (1984).
15. Ahmadi, G. and Goldschmidt, V. "Motion of particle in a turbulent fluid: The Basset history term," *J. Appl. Mech.*, ASME, **38**, pp 561-563 (1971).
16. Peskin, R.L. "Digital computer simulation of turbulent diffusion in advanced computer methods for partial differential equations," *Int. Assoc. for Math. and Computers in Simulations*, Rutgers Univ., New Brunswick, NJ, pp 207-214 (1975).
17. Ounis, H. and Ahmadi, G. "Motions of small rigid spheres in simulated random velocity field," *ASCE J. Eng. Mech.*, **115**, pp 2107-2121 (1989).
18. Ounis, H. and Ahmadi, G. "Analysis of dispersion of small spherical particles in a random velocity field," *J. Fluids Eng.*, **112**, pp 114-120 (1990).
19. Maxey, M.R. "The gravitational settling of aerosol particles in homogeneous turbulence and random flow fields," *Phys. Fluid*, **174**, pp 441-465 (1987).
20. McLaughlin, J.B. "Aerosol particle deposition in numerically simulated channel flow," *Phys. Fluids*, A, **1**, pp 1211-1224 (1989).
21. Ounis, H., Ahmadi, G. and McLaughlin, J.B. "Brownian diffusion of submicron particles in the viscous sublayer," *J. Colloid and Interface. Sci.*, **143**, pp 266-277 (1991).
22. Ounis, H., Ahmadi, G. and McLaughlin, J.B. "Dispersion and deposition of Brownian particles from point sources in a simulated turbulent channel flow," *J. Colloid and Interface. Sci.*, **147**, pp 233-250 (1991).
23. Rizk, M.A., and Elghobashi, S.E. "The motion of a spherical particle suspended in a turbulent flow near a plane wall," *Phys. Fluid*, **20**, pp 806-817 (1985).
24. Abuzeid, S., Busnaina, A.A. and Ahmadi, G. "Wall deposition of small suspended particles in a turbulent channel flow," submitted to *Particulate Sci. and Tech.*, (1989).
25. Abuzeid, S., Busnaina, A.A. and Ahmadi, G. "Wall deposition of aerosol particles in a turbulent channel flow," *J. of Aerosol Sciences.*, **22**, pp 43-62 (1991).
26. Li, A. and Ahmadi, G. "Dispersion and deposition of spherical particles from point sources in a turbulent channel flow," *J. Aerosol Sci. and Tech.*, **16**, pp 209-226 (1992).
27. Li, A. and Ahmadi, G. "Deposition of aerosols on surfaces in a turbulent channel flow," *Int. J. Eng. Sci.*, **31**, pp 435-451 (1993).

28. Li, A. and Ahmadi, G. "Computer simulation of deposition of aerosols in a turbulent channel flow with rough walls," Report No. MAE-235 June, Clarkson University, Potsdam, NY. Also in *Aerosol Sci. and Tech.*, **18**, pp 11-24 (1993).

29. Li, A., Ahmadi, G., Bayer, R.G. and Gaynes, M.A. "Aerosol particle dispersion and deposition in a complex geometry turbulent duct flow," Report No. MAE-249 March, Clarkson University, Potsdam, NY. Also in *J. Aerosol Sci. and Tech.* (in press) (1994).

30. Fān, F-G. and Ahmadi, G. "A sublayer model for turbulent deposition of particles in vertical ducts with smooth and rough surfaces," *J. Aerosol Sci. and Tech.*, **24**, pp 45-69 (1993).

31. Fan, F-G. and Ahmadi, G. "On the sublayer model for turbulent deposition of charged particles in the presence of electric fields," Report No. MAE-252 April, Clarkson University, Potsdam, NY (1992).

32. Saffman, P.G. "The lift on a small sphere in a slow shear flow," *J. Fluid Mech.*, **22**, pp 385-398 (1965).

33. Rodi, W. "A new algebric relation for calculating the Reynolds stresses," *ZAMM*, **56**, pp T219-T221 (1976).

34. Speziale, C.G. "On nonlinear K-l and K-ϵ models of turbulence," *J. Fluid Mech.*, **178**, pp 459-475 (1987).

35. Yoshizawa, A. *Phys. Fluids*, **27**, p 1377 (1984).

36. Yoshizawa, A. *Phys. Fluids*, **28**, p 59 (1985).

37. Ahmadi, G. and Chowdhury, S.J. "A rate-dependent algebraic stress model for turbulence," *Appl. Math. Modelling*, **15**, pp 516-524 (1991).

38. Ahmadi, G. "A thermodynamically consistent rate-dependent model for turbulence. Part I-Formulation," *Inter. J. Nonlinear Mech.* ,**26**, pp 595-607 (1991).

39. Chowdhury, S.J. and Ahmadi, G. "A thermodynamically consistent rate-dependent model for turbulence. Part II-Computational results," *Inter. J. Nonlinear Mech.*, **27**, pp 705-718 (1992).

40. Batchelor, G. K. *The Theory of Homogeneous Turbulence*, 2nd Edn., Cambridge University Press (1971).

41. Kraichnan, R. H. "Diffusion by random velocity field," *Phys. Fluid*, **11**, pp 22-31 (1970).

42. Kreplin, H.P. and Eckelmann, H. "Behavior of the three fluctuating velocity components in the wall region of a turbulent channel flow," *Phys. Fluids*, **22**, pp 1233-1239 (1979).

43. White, F.M. *Fluid Mechanics*, McGraw Hill, New York (1986).

44. Hinze, J.O. *Turbulence*, McGraw Hill, New York (1975).

45. Davies, J.T. *Turbulence Phenomena*, Academic Press, New York (1972).

46. Uhlenbeck, E.G. and Ornstein, S.L. "On the theory of the Brownian motion," *Physics Review*, **36**, pp 823-841 (1930).

47. Chandrasekhar, S. "Stochastic problems in physics and astronomy," *Reviews of Modern Physics*, **15**, pp 1-89 (1943).

48. Gupta, D. and Peters, M. "A Brownian dynamics simulation of aerosol deposition onto spherical collectors," *J. of Colloid and Interface Sci.*, **104** (1985).

49. Ounis, H. and Ahmadi, G. "A comparison of Brownian and turbulent diffusion," *J. of Aerosol Sci. and Tech.*, **13**, pp 47-53 (1990).

50. Reeks, M.W. *J. of Aerosol Sci. and Tech.*, **14**, pp 729-739 (1983).

51. Montgomery, T.L. and Corn, M. *J. of Aerosol Sci. and Tech.*, **1**, p 185 (1970).